


Mature osteoclast–derived apoptotic bodies promote osteogenic differentiation via RANKL-mediated reverse signaling

Received for publication, January 18, 2019, and in revised form, May 21, 2019. Published, Papers in Press, June 5, 2019. DOI 10.1074/jbc.RA119.007625

 Qinyu Ma^{†1},  Mengmeng Liang^{§1}, Yutong Wu[‡], Ning Ding[¶], Lianli Duan[‡], Tao Yu[‡], Yun Bai[‡], Fei Kang[§], Shiwu Dong[§], Jianzhong Xu^{‡2}, and  Ce Dou^{¶||3}

From the Departments of [†]Orthopedics and [§]Biomedical Materials Science, Southwest Hospital, Third Military Medical University, Chongqing 400038, China, the [¶]Department of Blood Purification, General Hospital of Shenyang Military Area Command, Shenyang 110000, China, and the ^{||}Department of Orthopedic Surgery, Johns Hopkins University School of Medicine, Baltimore, Maryland 21205

Edited by Xiao-Fan Wang

In bone remodeling, after a lifespan of ~2 weeks, osteoclasts undergo apoptosis in each bone turnover cycle, resulting in generation of a large number of apoptotic bodies (ABs). However, the biological roles of osteoclast-derived ABs (OC-ABs) in bone remodeling have not been investigated and remain unknown. In this study, we stimulated bone marrow macrophages with receptor activator of NF- κ B ligand (RANKL) to obtain both preosteoclasts and mature osteoclasts (mOCs). We then used alendronate to induce apoptosis in preosteoclasts and mOCs and generate the respective ABs and used flow cytometry and immunoblotting to characterize the sizes and immunogenic characteristics of the extracted ABs. We show that mOC-ABs are engulfed by preosteoblastic MC3T3-E1 cells and promote the viability of these cells. Among all osteoclast-derived extracellular vesicles, mOC-ABs had the highest osteogenic potency. We further observed that mOC-ABs had the highest vesicular receptor activator of NF- κ B (RANK) levels among all types of osteoclast-derived extracellular vesicles. Of note, masking of vesicular RANK by soluble RANKL strongly abolished the osteogenic potency of osteoclast-derived ABs. Mechanistically, we found that mOC-ABs induce osteoblast differentiation by activating PI3K/AKT/mechanistic target of rapamycin (mTOR)/ribosomal protein S6 kinase signaling. In conclusion, OC-ABs promote osteogenic differentiation by stimulating osteoblast differentiation via activation of RANKL reverse signaling. These findings provide important insights into the reversal phase between the bone resorption and formation stages during bone

remodeling and identify an AB-dependent cellular signaling mechanism in osteoclast–osteoblast coupling.

Bone remodeling is a lifelong process that involves the removal of bone tissue (bone resorption) by hematopoietic lineage osteoclasts, followed by the formation of bone matrix (bone formation) through mesenchymal lineage osteoblasts that subsequently become mineralized (1). Bone remodeling is accomplished by assembly of osteoclasts and osteoblasts into discrete temporary anatomic structures called basic multicellular units (2). The communication between osteoclasts and osteoblasts is termed “coupling” (3) and is later expanded to include more contributors such as osteocytes, macrophages, and T cells (4). Osteoclast–osteoblast coupling has long been of interest to understand how these two distinct cell types with different functioning periods during bone remodeling could be linked so their activities are equal in maintaining bone homeostasis (5). Compared with the well-studied effects of osteoblast-derived coupling factors in osteoclast differentiation and function, less is known about the converse osteoclast-derived messages and functions.

Two important regulating factors, receptor activator of NF- κ B ligand (RANKL)⁴ and macrophage colony stimulating factor (M-CSF) are necessary for osteoclast differentiation (6–8). RANKL is a transmembrane protein from the tumor necrosis factor superfamily; binding to its receptor RANK drives the central signaling pathway in preosteoclast (pOC) development and maintains the survival of mature osteoclasts (mOCs) (9). The average lifespan of human osteoclasts is relatively short, about 2 weeks, compared with the average lifespan of osteoblasts of 3 months (10, 11). At the end of its lifespan, the

This work was funded by the grant from the Nature Science Foundation of China (81802166), first class General Financial Grant from the China Postdoctoral Science Foundation (2017M613315), and TMMU funding for young investigators (2017MPRC-04), as well as postdoc training award (to CD) from the China Scholarship Council (CSC). The authors declare that they have no conflicts of interest with the contents of this article.

This article contains Figs. S1–S8, Table S1, and supporting Materials and Methods.

The RNA-Seq data reported in this paper were submitted to the GEO database with accession number GSE132230.

¹ Both authors contributed equally to this work.

² To whom correspondence may be addressed: Dept. of Orthopedics, Southwest Hospital, Third Military Medical University, Gaotanyan St. 30, Chongqing 400038, China. E-mail: xujianzhong1962@163.com.

³ To whom correspondence may be addressed: Dept. of Orthopedics, Southwest Hospital, Third Military Medical University, Gaotanyan St. 30, Chongqing 400038, China. E-mail: lance.douce@gmail.com.

⁴ The abbreviations used are: RANKL, receptor activator of NF- κ B ligand; M-CSF, macrophage colony-stimulating factor; RANK, receptor activator of NF- κ B; pOC, preosteoclast; mOC, mature osteoclast; AB, apoptotic body; EV, extracellular vesicle; BMM, bone marrow macrophage; ALN, alendronate; TRAP, tartrate-resistant acid phosphatase; FCM, flow cytometry; CM, conditioned medium; ABRM, apoptotic body–rich medium; MV, microvesicle; Exo, exosome; WB, Western blot; MFI, mean fluorescence intensity; ALP, alkaline phosphatase; mTOR, mechanistic target of rapamycin; PI, propidium iodide; sRANKL, soluble RANKL; GO, gene ontology; KEGG, Kyoto encyclopedia of genes and genomes; ACTB, actin-beta.

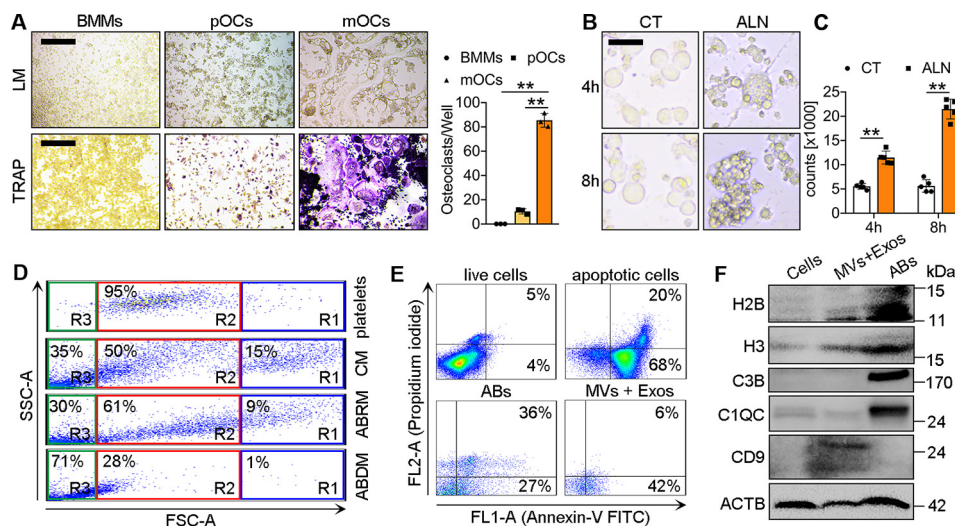


Figure 1. ALN stimulates the generation of osteoclast-derived ABs. *A*, light microscopy (LM) and TRAP stain of BMMs, pOCs, and mOCs stimulated with sRANKL. *Right panel*, quantification analysis of osteoclast number per well ($n = 3$). Scale bars = 100 μm . *B*, mOCs were induced with ALN (500 μM) and observed using light microscopy 4 and 8 h after induction. Scale bar = 20 μm . mOC treated with ALN are defined as control (CT) group. *C*, quantification of subcellular fragment counts ($n = 5$). *D*, forward scatter (FSC)/side scatter (SSC) dot plot analysis of particles from apoptotic mOCs. Platelets were used as a size marker (1–4 μm , red, gate R2). Conditioned medium from apoptotic mOCs contained dead cells and large cell debris (green, gate R1), ABs (gate R2), and MVs and Exos (blue, gate R3). ABRM, obtained after centrifugation ($800 \times g$, 10 min), contained mainly ABs, MVs, and Exos. AB-depleted medium (ABDM), obtained after centrifugation ($16,000 \times g$, 20 min) of the ABRM, contained mainly MVs and Exos. The percentage of events is given in the top left corner of each region gate. *E*, Annexin V/FITC (FL1-A) and PI (FL2-A) dot plot analysis of live cells, dead cells, ABs, and MVs and Exos. The quadrant gates were set on the respective unstained control population. The percentage of events is given in the top right corner of the respective region. *F*, Western blot analysis of H2B, H3, C3B, C1QC, CD9, and ACTB in extracted ABs. The data represent averages \pm S.D. Significant differences are indicated as follows: *, $p < 0.05$; **, $p < 0.01$; paired using Student's *t* test unless otherwise specified.

osteoclast undergoes apoptosis, a kind of programmed cell death characterized by nuclear and cytoplasmic condensation and formation of plasma and nuclear membrane blebs (12). Eventually the cell breaks apart to form apoptotic bodies (ABs).

ABs are a major class of extracellular vesicles (EVs) released as a product of apoptotic cell disassembly. This separates ABs from other types of EVs, such as exosomes and microvesicles, which are constantly generated by normal viable cells (13). AB size ranges from 1000–5000 nm, comparable with normal platelets (14). The content of ABs is variable and may include nucleic acids, proteins, and lipids (15, 16). Some autoantigens are also translocated into ABs during AB formation including the histone family, complement C1q C chain (C1QC), and complement component 3B (C3B), specific markers of ABs (13). Less is known about the underlying mechanisms of AB formation compared with other types of EVs; recent studies suggest that it is a highly regulated process mediated by actomyosin contraction–controlled membrane protrusion (17). Accumulating evidence supports the importance of ABs in immune modulation and related disease settings. Therefore, ABs are more than just debris or by-products of apoptosis and should be considered a key mechanism for apoptotic cells to communicate with surrounding cells (18). So far, the function of osteoclast-derived ABs in basic multicellular units and bone remodeling has not been investigated and remains unknown.

In this study, we investigated the effects of bone marrow macrophage (BMM)-ABs, pOC-ABs, and mOC-ABs in osteogenic differentiation of preosteoblastic MC3T3-E1 cells. mOC-ABs exhibited the best osteogenic activity by activating RANKL reverse signaling. These findings suggest an important regulatory role of osteoclast-derived ABs in osteogenic differentiation and bone remodeling.

Results

ALN stimulates generation of osteoclast-derived ABs

We used nitrogen-containing bisphosphonate alendronate (ALN) to induce apoptosis of BMMs, pOCs, and mOCs to generate ABs (19, 20). BMMs were isolated and induced with RANKL to obtain pOCs (0–48 h after RANKL stimulation) and mOCs (60–120 h after RANKL stimulation), confirmed by tartrate-resistant acid phosphatase (TRAP) staining and quantification of osteoclast numbers (Fig. 1A). Light microscopy analyses of viable and apoptotic cells were performed to confirm apoptotic induction of ALN after 4 and 8 h of incubation of BMMs (Fig. S1), pOCs (Fig. S2), and mOCs (Fig. 2B). Cell apoptosis induced by ALN was confirmed by increased formation of subcellular fragments (Fig. 2C) and detected by flow cytometry (FCM) (Fig. S3). ABs were then analyzed by FCM using forward/side scatter dot plot analysis. We analyzed and compared conditioned medium (CM) from apoptotic cells without centrifugation, after centrifugation of CM at $800 \times g$ for 10 min for removal of dead cells and large cell debris to obtain AB-rich medium (ABRM), and after centrifugation at $16,000 \times g$ for 20 min of ABRM for removal of ABs to obtain AB-depleted medium. Platelets were used for size comparison (1–4 μm , Fig. 1D). ABs are approximately in the size range of platelets (1–4 μm), whereas microvesicles (MV) and exosomes (Exos) are much smaller ($<1 \mu\text{m}$). Annexin V/FITC staining showed that apoptotic cells, ABs, MVs, and Exos are positive for Annexin V (Fig. 1E). In contrast, staining with PI showed that ABs, but not MVs and Exos, are positive for PI (Fig. 1E). For further characterization, Western blot (WB) analysis was performed, and the results showed that ABs contain increased AB markers, including histone 2B (H2B), histone 3 (H3), C3B, and C1QC, and lack

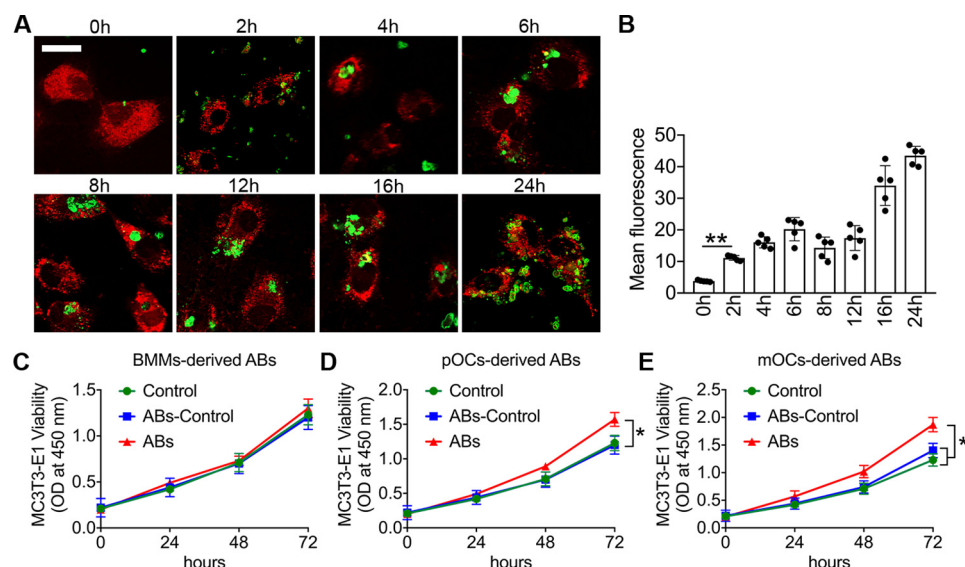


Figure 2. ABs are engulfed by recipient MC3T3-E1 cells. A, MC3T3-E1 cells (stained with Cell Tracker Red) were co-incubated with Annexin V/FITC-labeled ABs (cultured for 24 h). Scale bar = 20 μ m. B, quantification of the mean fluorescence intensity of engulfed ABs by MC3T3-E1 cells after co-incubation ($n = 5$). C–E, cell viability evaluation of MC3T3-E1 cells co-incubated with BMM-ABs (C), pOC-ABs (D), and mOC-ABs (E) using a CCK8 test at 0, 24, 48, and 72 h ($n = 5$). ABs-Control, ABs derived from RAW264.7 cells. The data represent averages \pm S.D. Significant differences are indicated as follows: *, $p < 0.05$; **, $p < 0.01$; paired using Student's t test unless otherwise specified.

the MV and Exo marker CD9 (Fig. 1F). We obtained BMM-ABs, pOC-ABs, and mOC-ABs with ALN induction and further characterized the obtained ABs with FCM and WB analysis regarding sizes and specific markers.

ABs are engulfed by recipient MC3T3-E1 cells

ABs labeled with Annexin V/FITC were co-incubated with cell tracker CM-Dil-labeled live MC3T3-E1 cells to analyze the engulfment of ABs by the latter. Confocal microscopy was performed to analyze the co-culture of ABs and MC3T3-E1 cells (Fig. 2A). ABs were found outside of cells at 0 h. With prolonged incubation time, a marked increase in AB engulfment into the cells was observed. Gating on MC3T3-E1 cells, we analyzed the mean fluorescence intensity (MFI) after the indicated incubation periods (Fig. 2B). The results showed a significant increase in mean fluorescence at 2 h (gating on MC3T3-E1 cells), indicating engulfment of Annexin V/FITC-labeled ABs. We further detected effects of BMM-ABs, pOC-ABs, and mOC-ABs on recipient MC3T3-E1 cell viability. ABs derived from BMMs showed no significant change in viability of MC3T3-E1 cells compared with controlled ABs derived from RAW264.7 cells (Fig. 2C). However, ABs from both pOCs and mOCs significantly increased MC3T3-E1 cell viability after 72-h co-incubation (Fig. 2, D and E). The results suggested that ABs were engulfed and accumulated in a time-dependent manner by MC3T3-E1 cells. In addition, ABs derived from both pOCs and mOCs increased the viability of preosteoblastic MC3T3-E1 cells.

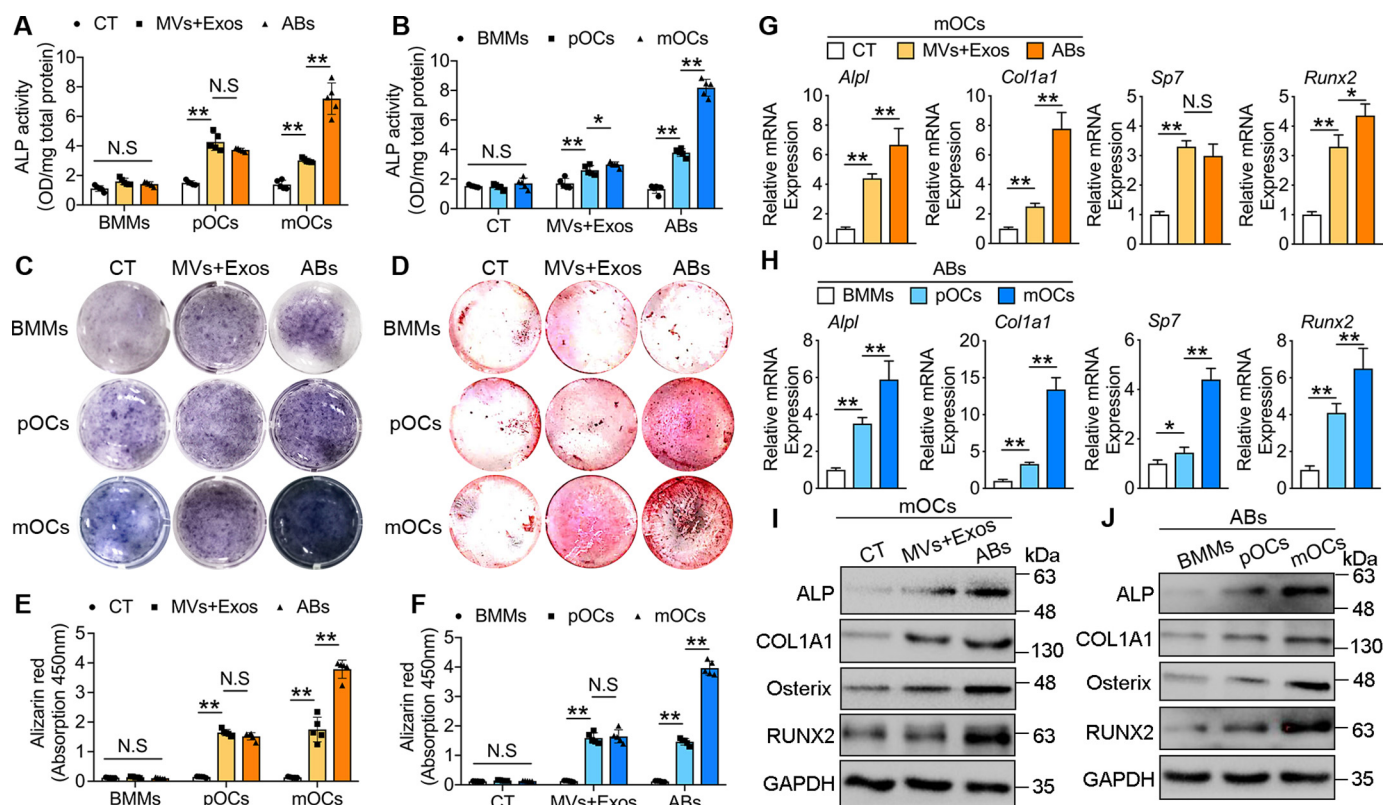
mOC-ABs have the highest osteogenic potency

To compare the osteogenic potency of MVs, Exos, and ABs, we tested the alkaline phosphatase (ALP) activity of MC3T3-E1 cells co-cultured with MVs and Exos or ABs derived from BMMs, pOCs, and mOCs. Quantification analysis revealed that MVs, Exos, and ABs derived from osteoclasts (pOCs and

mOCs) have osteogenic potency, but not those derived from BMMs. MVs, Exos, and ABs derived from pOCs showed no significant difference in osteogenic potency. However, in mOC-derived EVs, mOC-ABs showed significantly higher osteogenic potency compared with mOC-MVs and mOC-Exos (Fig. 3A). We further showed that MVs, Exos, and ABs derived from mOCs have better osteogenic potency compared with those derived from pOCs (Fig. 3B). ALP staining (Fig. 3C) and Alizarin Red staining (Fig. 3D) showed consistent results suggesting the highest mineralization of MC3T3-E1 cells co-cultured with mOC-derived ABs (Fig. 3, E and F). Similarly, qPCR results showed the highest up-regulation of the osteogenic regulators Runt-related transcription factor 2 (*Runx2*) and Osterix (*OSX*, also known as *Sp7*) together with the osteogenic markers type I collagen (*Col1a1*) and *Alpl* in the mOC-AB group among mOC-derived EVs (Fig. 3G). Among ABs derived from different cell types, mOC-ABs showed the highest up-regulation of *Runx2*, *Sp7*, *Col1a1*, and *Alpl* (Fig. 3H). On the protein level, WB analysis confirmed up-regulation of ALP, COL1A1, Osterix, and RUNX2 by mOC-AB treatment in MC3T3-E1 cells (Fig. 3, I and J). We also used mesenchymal stem cells for verification, and the results were similar with MC3T3-E1 cells (Fig. S4). Together, the above results suggest that mOC-derived EVs have better osteogenic potency, whereas mOC-ABs showed the best osteogenic potency among mOC-derived EVs.

Vesicular RANK masking by sRANKL reduced osteogenic potency

Inspired by the very recent discovery of the crucial role of RANKL reverse signaling in the coupling of bone resorption and formation (21), we detected the RANK expression level among mOC-derived EVs and found that mOC-ABs showed the highest level of RANK (Fig. 4A). Moreover, ABs derived from mOCs showed the highest RANK level compared with BMMs and pOCs (Fig. 4B). Furthermore, we found that mask-



ing of vesicular RANK by preincubation of ABs with sRANKL abolished the osteogenic effects of both pOC-ABs and mOC-ABs characterized by reduced ALP activity (Fig. 4, **C** and **E**) and mineralization (Fig. 4, **D** and **F**). Consistently, mOC-AB-upregulated expression of *Runx2*, *Sp7*, *Col1a1*, and *Alpl* was decreased by vesicular RANK masking (Fig. 4G). On the protein level, WB analysis confirmed the abolishment of vesicular RANK masking in mOC-AB osteogenic potency, marked by reduced expression of ALP, COL1A1, Osterix, and RUNX2 (Fig. 4I). Together, the results suggest that osteoclast-derived ABs stimulate osteogenic differentiation mainly by vesicular RANK.

RANKL reverse signaling contributes to the osteogenic potency of mOC-derived ABs

We found that activation of RUNX2 by mOC-ABs was remarkably reduced by pretreatment with the mechanistic target of rapamycin complex 1 (mTORC1) inhibitor rapamycin and masking of vesicular RANK by sRANKL (Fig. 5A). To explore the intracellular signaling pathways involved in RUNX2 activation, we examined the major mTORC1 upstream signaling molecules PI3K and Akt and the downstream molecule S6K in MC3T3-E1 cells treated with mOC-ABs. Cells were preincubated with mOC-ABs or mOC-ABs and sRANKL for vesicular RANK masking or mOC-ABs and rapamycin for

mTORC1 inhibition. Phosphorylation of PI3K, Akt, and S6K was detected 30 min (Fig. 5B), 60 min (Fig. 5C), or 120 min (Fig. 5D) after osteogenic stimulation. The results showed that vesicular RANK masking by sRANKL inhibited the activation of both PI3K, Akt, and S6K, whereas rapamycin only inhibited the activation of S6K. These results suggested that mOC-ABs stimulate osteogenic differentiation by activating RANKL reverse signaling.

To better understand the contents of pOC-ABs and mOC-ABs, we performed RNA-Seq to profile the mRNA contained in ABs derived from different stages of osteoclasts (Fig. S5). The data are documented in the GEO database with accession number GSE132230. Most differentially expressed mRNAs were presented separately (Fig. S6) together with the GO and KEGG analysis (Figs. S7 and S8). These data serve as a potential reservoir for researchers interested in further low-throughput validation and study of molecules of interests in the future.

Discussion

Apoptosis is a highly regulated programmed cell death process that plays a critical role not only in embryonic development but also in cell homeostasis in adults. Apoptosis is involved in almost all diseases, from cancer to neurological and cardiovascular disorders (22). Osteoclast apoptosis has also been identified to regulate bone homeostasis and bone disorder

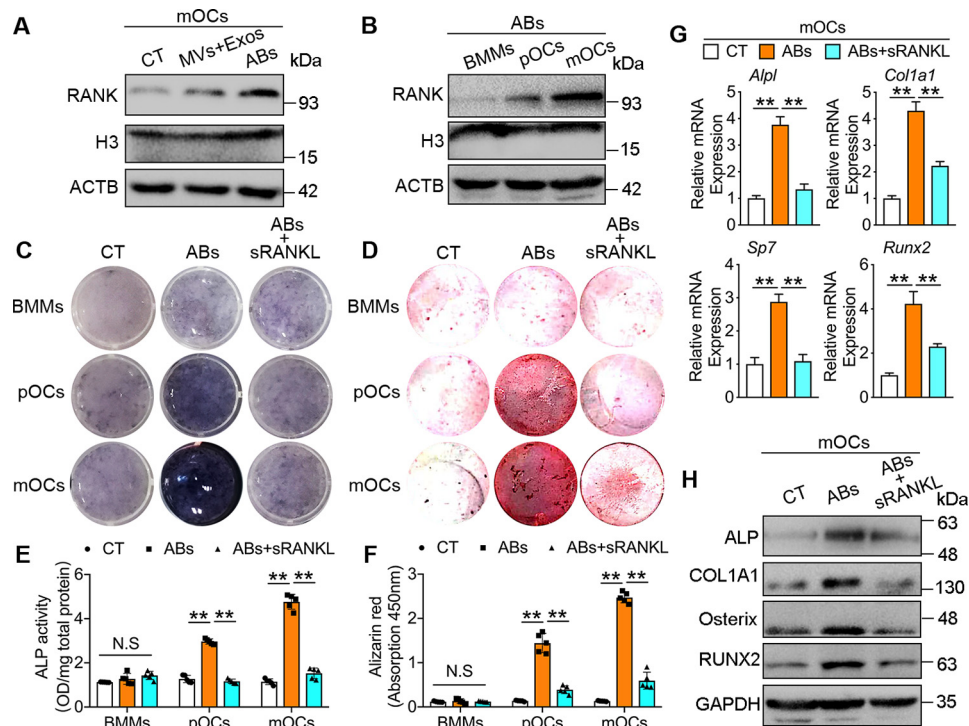


Figure 4. Vesicular RANK masking by sRANKL reduced osteogenic potency. A, Western blot analysis of RANK, H3, and ACTB in mOC-derived MVs, Exos, and ABs. ABs derived from BMMs are defined as control (CT) groups. B, Western blot analysis of RANK, H3, and ACTB in ABs derived from BMMs, pOCs, and mOCs. C and D, ALP stain (C) and Alizarin Red stain (D) of MC3T3-E1 cells treated with ABs derived from BMMs, pOCs, and mOCs with or without masking of vesicular RANK by sRANKL. E, quantification of ALP activity in C. F, quantification of Alizarin Red stain in D. G, relative mRNA expression levels of *Alpl*, *Col1a1*, *Sp7*, and *Runx2* in MC3T3-E1 cells treated with mOC-derived ABs with or without masking of vesicular RANK by sRANKL. H, Western blot analysis of ALP, COL1A1, Osterix, Runx2, and GAPDH in MC3T3-E1 cells treated with mOC-derived ABs with or without masking of vesicular RANK by sRANKL. The data represent averages \pm S.D. Significant differences are indicated as follows: *, $p < 0.05$; **, $p < 0.01$; paired using Student's *t* test unless otherwise specified. N.S., not significant.

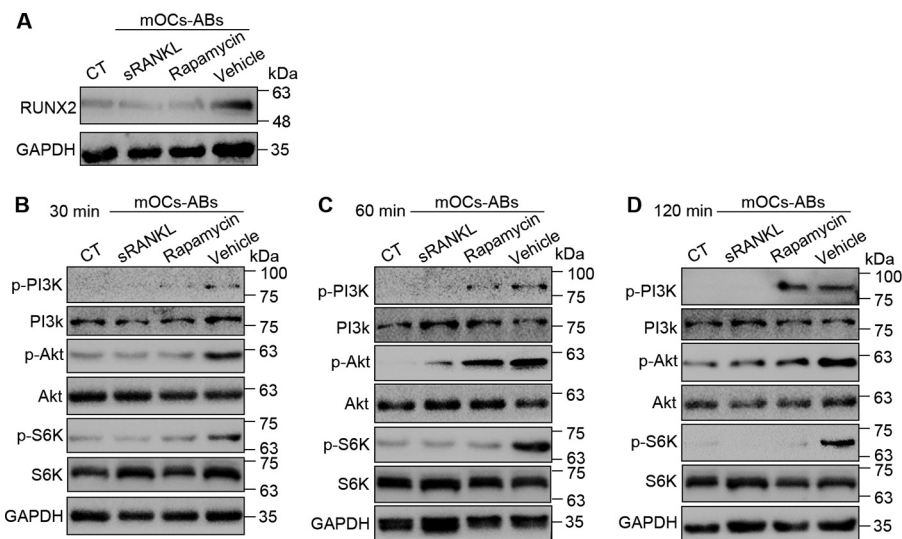


Figure 5. RANKL reverse signaling contributes to the osteogenic potency of mOC-ABs. A, Western blot analysis of RUNX2 and GAPDH in MC3T3-E1 cells treated with mOC-ABs, sRANKL-preincubated mOC-ABs, or mOC-ABs with rapamycin. MC3T3-E1 cells treated with α -MEM without MVs and Exos or ABs are defined as control (CT) groups. B–D, Western blot analysis of p-PI3K, PI3K, p-Akt, Akt, p-S6K, S6K, and GAPDH in MC3T3-E1 cells treated with mOC-ABs, sRANKL-preincubated mOC-ABs, or mOC-ABs with rapamycin at 30 min (B), 60 min (C), and 120 min (D).

ders (23, 24). In osteoclast–osteoblast coupling, apoptosis of osteoclasts has long been considered a consequence induced by osteoblasts (25, 26). However, researchers rarely investigated the converse effects of osteoclast apoptosis in osteoblastic activities. In this study, for the first time, we showed that ABs derived from osteoclasts possess osteogenic potency by activating RANKL reverse signaling in preosteoblasts (Fig. 6). Fur-

thermore, mOC-ABs showed the highest osteogenic potency among osteoclast-derived EVs. It should be noted that, although mOC-ABs are significantly different from pOC-ABs because of the generation of large multinucleated mOCs, pOCs cannot be fully depleted in mOC culture. Therefore, mOC-ABs might not be as pure as we think and may include a fraction of pOC-ABs, which is a limitation of this study.

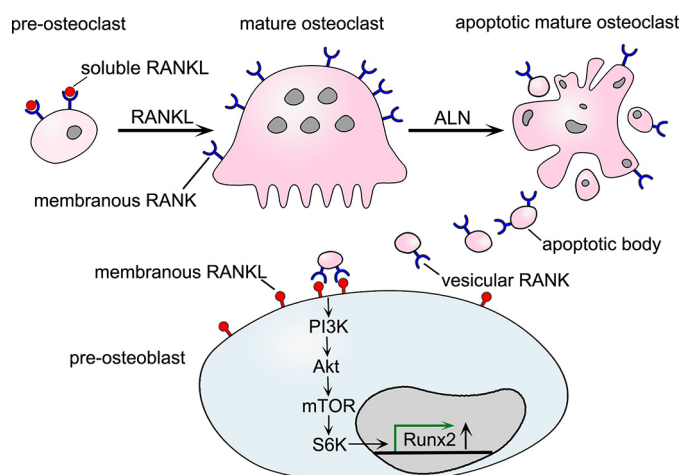


Figure 6. Schematic of RANKL reverse signaling activation by mOC-ABs. pOCs are stimulated by soluble RANKL and differentiate into mOCs. ALN is used to induce apoptosis of mOCs in generation of mOC-ABs. Vesicular RANK of mOC-ABs binds to membranous RANKL of preosteoblasts to activate RANKL reverse signaling in a sequence of PI3K–Akt–mTOR–S6K and further increases transcription of *Runx2* to promote osteogenic differentiation.

RANKL reverse signaling was recently identified and described by Ikebuchi *et al.* (21) as an important coupling mechanism of bone resorption and formation. In their study, small extracellular vesicles secreted by mOCs were identified to stimulate osteoblast differentiation via vesicular RANK-mediated RANKL reverse signaling. In our study, we further detected osteogenic effects of ABs from both pOCs and mOCs compared with MVs and exosomes derived from each cell. Interestingly, we found that ABs, especially mOC-ABs, showed the highest osteogenic potency among all osteoclast-derived EVs. Mechanistically, mOC-ABs also function through RANKL reverse signaling. In this way, the highest vesicular RANK expression level of mOC-ABs explained its best osteogenic potency among OC-EVs.

ABs play a central role in the interaction of a dying cell with the immune system as well as in mediating intercellular communication (27). The immunomodulatory roles of ABs have been described in antigen presentation (28), antitumor immunity (28), antimicrobial immunity (29), and autoimmunity (30). In the skeletal system, a role of ABs has rarely been reported. We observed engulfment of ABs by preosteoclasts, supported by a previous report in which osteoblasts were observed to be capable of engulfing ABs during alveolar bone formation (31). Early work also reported that osteoclast-derived ABs are engulfed by macrophages *in vivo* (32), indicating the exciting possibility that osteoclast may regulate self-differentiation by affecting osteoclast precursor differentiation by generating ABs.

Human physical bone turnover consists of three phases: bone resorption mediated by osteoclasts of ~3 weeks (33), bone formation and mineralization of about 3–4 months (34), and a reversal phase of ~5 weeks between bone resorption and formation, which is poorly understood (35). Cell coupling between osteoclasts and osteoblasts may dominate this time delay between bone resorption and formation. It is recognized that osteoblast progenitors are capable of sensing osteoclast-derived factors either released from the matrix, secreted from the

osteoclast, or expressed on the osteoclast cell membrane to initiate differentiation (5). However, it remains unknown whether and how apoptotic osteoclasts emerge at the end of the bone resorption phase, and the subsequent generation of a vast number of ABs may further influence the upcoming bone formation phase in the whole bone turnover process. Our study filled this gap by showing and proving the strong osteogenic potency of osteoclast-derived ABs.

In summary, our study revealed stimulatory effects of ABs derived from osteoclasts in osteoblast differentiation. Furthermore, we showed that mOC-ABs have the best osteogenic potency among all types of OC-derived EVs because of the highest expression of vesicular RANK and the subsequent activation of RANKL reverse signaling.

Experimental procedures

Osteoclast differentiation assay

Bone marrow cells were separated and cultured with M-CSF (50 ng/ml) for 24 h to obtain BMMs. Cells were cultured in α -minimal essential medium containing 10% FBS and 1% penicillin–streptomycin solution. For TRAP staining, cells were cultured in a 96-well plate at a density of 5×10^3 cells/well with RANKL (100 ng/ml) and M-CSF (50 ng/ml) for 3 days. Cells were fixed in 4% paraformaldehyde for 20 min and then stained with TRAP staining solution (0.1 mg/ml of naphthol phosphate disodium salt, 0.3 mg/ml of Fast Red Violet zinc chloride stain) according to the manufacturers' instructions. Relative TRAP activity was measured by colorimetric analysis.

AB generation and extraction

Cell apoptosis was induced by treatment with ALN (500 μ M) for 24 h at 37 °C. ALN was obtained from Med Chem Express. ABs were isolated using sequential centrifugation and sequential filtration. In short, supernatant was collected from wells that cultured apoptotic cells and centrifuged at $300 \times g$ for 10 min to remove cell debris. Subsequently, the supernatant was filtered with 1- and 5- μ m filters to limit particle diameter to 1–5 μ m. Next, the supernatant was centrifuged at $3500 \times g$ for 20 min to pellet the AB-sized extracellular vesicles. AB-sized extracellular vesicles derived from osteoclasts and ALN-treated OCs were isolated after subsequent centrifugation and then stained with Annexin V/FITC in 500 μ l of binding buffer (30 min at 21 °C). AB-sized extracellular vesicles were pelleted again to remove binding buffer for identification and analysis.

Flow cytometry

Flow cytometry analyses were performed using a BD Accuri C6 flow cytometer, counting at least 10,000 events. After extraction and staining, AB-sized extracellular vesicles were resuspended in 500 μ l of PBS. Cell apoptosis was determined by Annexin V/PI staining as described previously (36). In brief, cells were stained with Annexin V/FITC (Life Technologies) and PI. Viable cells were negative for both Annexin V and PI. Early apoptotic (still viable) cells were positive for Annexin V and negative for PI. Late apoptotic (nonviable) cells were positive for Annexin V and PI. Necrotic cells were positive for PI and negative for Annexin V.

mOC-ABs induce osteoblast differentiation

AB identification and calculation

After extraction, ABs were stained with 50 mg/ml PI and 20 mg/ml Annexin V/FITC for 30 min at 37 °C in 500 μ l of binding buffer. PI is used to determine nuclear granularity and hypochromicity, and Annexin V/FITC is used to detect phosphatidylserine exposure on the cell surface. Here we used an apoptosis assay kit obtained from Sigma. Then cells were immediately analyzed by flow cytometry to quantify the rate of apoptosis.

AB engulfment assay and MFI analysis

After being isolated from cellular supernatants, ABs were stained with Annexin V/FITC (50 mg/ml) for 30 min at 21 °C. MC3T3-E1 cells were labeled with Cell Tracker Red for 30 min at 21 °C. Annexin V/FITC-labeled ABs were coincubated with Cell Tracker Red-labeled MC3T3-E1 cells for 24 h. After the full incubation time according to group settings, ABs that were not engulfed by cells were washed away using 1 \times PBS and then observed using confocal microscopy to verify AB ingestion. Gating on MC3T3-E1 cells, FITC fluorescence was analyzed by flow cytometry. Flow cytometry was performed using a BD Accuri C6 flow cytometer, counting at least 20,000 events. MFI was calculated and generated using Flowjo-V10 software.

Osteogenic differentiation assay

MC3T3-E1 cells were loaded at 1 \times 10⁶ cells/well into a 24-well plate. We started to induce osteogenic differentiation when cells reached 100% contact and stopped proliferating. MC3T3-E1 cells were cultured in osteogenic medium consisting of 2 mM β -glycerophosphate (Aladdin), 100 μ M ascorbic acid 2-phosphate (Aladdin), and 10 nM dexamethasone (Aladdin). 3, 5, and 7 days after osteogenic induction, total protein was extracted from cultured MC3T3-E1 cells, and the expression of osteoblastic markers was assayed by immunoblotting analysis. To assess ALP activity, MC3T3-E1 cells were fixed in 4% paraformaldehyde and then treated according to the protocol for the alkaline phosphatase assay kit (Beyotime Biotechnology) after a week of osteogenic induction. To assess the deposition of calcium ions, MC3T3-E1 cells were fixed in 4% paraformaldehyde and then stained with 1% Alizarin Red S (Solarbio Life Sciences).

quantitative RT-PCR

Total RNA was isolated using TRIzol reagent (Life Technologies). Single-stranded complementary DNA was prepared from 1 μ g of total RNA using reverse transcriptase with an oligo(dT) primer according to the manufacturer's instructions (Promega). Two microliters of each complementary DNA were subjected to PCR amplification using specific primers (Table S1).

Immunoblotting

Cells were lysed in lysis buffer containing 10 mM Tris (pH 7.2), 150 mM NaCl, 5 mM EDTA, 0.1% SDS, 1% Triton X-100, and 1% deoxycholic acid. For western blotting, 30 μ g of protein samples were subjected to SDS-PAGE, followed by transfer onto PVDF membranes. After blocking in 5% skim milk, the membranes were incubated with rabbit antibodies against pri-

mary antibodies overnight at 4 °C, followed by 1-h incubation with a secondary antibody.

Statistical analysis

All data are representative of at least three experiments with similar results performed in triplicate unless otherwise indicated. Data are expressed as mean \pm S.D. One-way analysis of variance followed by Student–Newman–Keuls post hoc test was used to determine the significance of difference between results, with *, $p < 0.05$ and **, $p < 0.01$ regarded as significant.

Author contributions—Q. M. and Y. B. formal analysis; Q. M., M. L., and T. Y. supervision; Q. M., M. L., Y. W., N. D., L. D., and F. K. investigation; Q. M. and L. D. methodology; M. L., S. D., and C. D. data curation; M. L. software; M. L. project administration; N. D., J. X., and C. D. visualization; N. D. and J. X. writing-original draft; T. Y. resources; Y. B. validation; F. K. funding acquisition; S. D., J. X., and C. D. writing-review and editing; J. X. and C. D. conceptualization.

References

1. Hadjidakis, D. J., and Androulakis, I. I. (2006) Bone remodeling. *Ann. N.Y. Acad. Sci.* **1092**, 385–396 [CrossRef Medline](#)
2. Jilka, R. L. (2003) Biology of the basic multicellular unit and the pathophysiology of osteoporosis. *Med. Pediatr. Oncol.* **41**, 182–185 [CrossRef Medline](#)
3. Howard, G. A., Bottemiller, B. L., Turner, R. T., Rader, J. I., and Baylink, D. J. (1981) Parathyroid hormone stimulates bone formation and resorption in organ culture: evidence for a coupling mechanism. *Proc. Natl. Acad. Sci. U.S.A.* **78**, 3204–3208 [CrossRef Medline](#)
4. Sims, N. A., and Gooi, J. H. (2008) Bone remodeling: multiple cellular interactions required for coupling of bone formation and resorption. *Semin. Cell Dev. Biol.* **19**, 444–451 [Medline](#)
5. Sims, N. A., and Martin, T. J. (2015) Coupling signals between the osteoclast and osteoblast: how are messages transmitted between these temporary visitors to the bone surface? *Front. Endocrinol.* **6**, 41 [Medline](#)
6. Boyle, W. J., Simonet, W. S., and Lacey, D. L. (2003) Osteoclast differentiation and activation. *Nature* **423**, 337–342 [CrossRef Medline](#)
7. Yasuda, H., Shima, N., Nakagawa, N., Yamaguchi, K., Kinosaki, M., Mochizuki, S., Tomoyasu, A., Yano, K., Goto, M., Murakami, A., Tsuda, E., Morinaga, T., Higashio, K., Udagawa, N., Takahashi, N., and Suda, T. (1998) Osteoclast differentiation factor is a ligand for osteoprotegerin/osteoclastogenesis-inhibitory factor and is identical to TRANCE/RANKL. *Proc. Natl. Acad. Sci. U.S.A.* **95**, 3597–3602 [CrossRef Medline](#)
8. Lacey, D. L., Timms, E., Tan, H. L., Kelley, M. J., Dunstan, C. R., Burgess, T., Elliott, R., Colombero, A., Elliott, G., Scully, S., Hsu, H., Sullivan, J., Hawkins, N., Davy, E., Capparelli, C., et al. (1998) Osteoprotegerin ligand is a cytokine that regulates osteoclast differentiation and activation. *Cell* **93**, 165–176 [CrossRef Medline](#)
9. Kong, Y. Y., Yoshida, H., Sarosi, I., Tan, H. L., Timms, E., Capparelli, C., Morony, S., Oliveira-dos-Santos, A. J., Van, G., Itie, A., Khoo, W., Wakeham, A., Dunstan, C. R., Lacey, D. L., Mak, T. W., et al. (1999) OPG is a key regulator of osteoclastogenesis, lymphocyte development and lymph-node organogenesis. *Nature* **397**, 315–323 [CrossRef Medline](#)
10. Manolagas, S. C. (2000) Birth and death of bone cells: basic regulatory mechanisms and implications for the pathogenesis and treatment of osteoporosis. *Endocr. Rev.* **21**, 115–137 [CrossRef Medline](#)
11. Marks, S. C., Jr., and Seifert, M. F. (1985) The lifespan of osteoclasts: experimental studies using the giant granule cytoplasmic marker characteristic of beige mice. *Bone* **6**, 451–455 [CrossRef Medline](#)
12. Steller, H. (1995) Mechanisms and genes of cellular suicide. *Science* **267**, 1445–1449 [CrossRef Medline](#)
13. Akers, J. C., Gonda, D., Kim, R., Carter, B. S., and Chen, C. C. (2013) Biogenesis of extracellular vesicles (EV): exosomes, microvesicles, retrovirus-like vesicles, and apoptotic bodies. *J. Neurooncol.* **113**, 1–11 [CrossRef Medline](#)

14. Hristov, M., Erl, W., Linder, S., and Weber, P. C. (2004) Apoptotic bodies from endothelial cells enhance the number and initiate the differentiation of human endothelial progenitor cells *in vitro*. *Blood* **104**, 2761–2766 [CrossRef Medline](#)
15. Bergsmedh, A., Szeles, A., Henriksson, M., Bratt, A., Folkman, M. J., Spetz, A. L., and Holmgren, L. (2001) Horizontal transfer of oncogenes by uptake of apoptotic bodies. *Proc. Natl. Acad. Sci. U.S.A.* **98**, 6407–6411 [CrossRef Medline](#)
16. Zernecke, A., Bidzhekov, K., Noels, H., Shagdarsuren, E., Gan, L., Denecke, B., Hristov, M., Köppel, T., Jahantigh, M. N., Lutgens, E., Wang, S., Olson, E. N., Schober, A., and Weber, C. (2009) Delivery of microRNA-126 by apoptotic bodies induces CXCL12-dependent vascular protection. *Sci. Signal.* **2**, ra81 [Medline](#)
17. Atkin-Smith, G. K., Tixeira, R., Paone, S., Mathivanan, S., Collins, C., Liem, M., Goodall, K. J., Ravichandran, K. S., Hulett, M. D., and Poon, I. K. (2015) A novel mechanism of generating extracellular vesicles during apoptosis via a beads-on-a-string membrane structure. *Nat. Commun.* **6**, 7439 [CrossRef Medline](#)
18. Caruso, S., and Poon, I. K. H. (2018) Apoptotic cell-derived extracellular vesicles: more than just debris. *Front. Immunol.* **9**, 1486 [CrossRef Medline](#)
19. Ding, N., Liu, C., Yao, L., Bai, Y., Cheng, P., Li, Z., Luo, K., Mei, T., Li, J., Xing, J., Gao, X., Ma, Q., Xu, J., Luo, F., and Dou, C. (2018) Alendronate induces osteoclast precursor apoptosis via peroxisomal dysfunction mediated ER stress. *J. Cell. Physiol.* **233**, 7415–7423 [CrossRef Medline](#)
20. Drake, M. T., Clarke, B. L., and Khosla, S. (2008) Bisphosphonates: mechanism of action and role in clinical practice. *Mayo Clin. Proc.* **83**, 1032–1045 [CrossRef Medline](#)
21. Ikebuchi, Y., Aoki, S., Honma, M., Hayashi, M., Sugamori, Y., Khan, M., Kariya, Y., Kato, G., Tabata, Y., Penninger, J. M., Udagawa, N., Aoki, K., and Suzuki, H. (2018) Coupling of bone resorption and formation by RANKL reverse signalling. *Nature* **561**, 195–200 [CrossRef Medline](#)
22. Favaloro, B., Allocati, N., Graziano, V., Di Ilio, C., and De Laurenzi, V. (2012) Role of apoptosis in disease. *Aging* **4**, 330–349 [CrossRef Medline](#)
23. Hughes, D. E., and Boyce, B. F. (1997) Apoptosis in bone physiology and disease. *Mol. Pathol.* **50**, 132–137 [CrossRef Medline](#)
24. Boyce, B. F., Wright, K., Reddy, S. V., Koop, B. A., Story, B., Devlin, R., Leach, R. J., Roodman, G. D., and Windle, J. J. (1995) Targeting simian virus 40 T antigen to the osteoclast in transgenic mice causes osteoclast tumors and transformation and apoptosis of osteoclasts. *Endocrinology* **136**, 5751–5759 [CrossRef Medline](#)
25. Wang, L., Liu, S., Zhao, Y., Liu, D., Liu, Y., Chen, C., Karray, S., Shi, S., and Jin, Y. (2015) Osteoblast-induced osteoclast apoptosis by fas ligand/FAS pathway is required for maintenance of bone mass. *Cell Death Differ.* **22**, 1654–1664 [CrossRef Medline](#)
26. Garcia, A. J., Tom, C., Guemes, M., Polanco, G., Mayorga, M. E., Wend, K., Miranda-Carboni, G. A., and Krum, S. A. (2013) ER α signaling regulates MMP3 expression to induce FasL cleavage and osteoclast apoptosis. *J. Bone Miner. Res.* **28**, 283–290 [CrossRef Medline](#)
27. Martin, S., Tesse, A., Hugel, B., Martínez, M. C., Morel, O., Freyssinet, J. M., and Andriantsitohaina, R. (2004) Shed membrane particles from T lymphocytes impair endothelial function and regulate endothelial protein expression. *Circulation* **109**, 1653–1659 [CrossRef Medline](#)
28. Zirngibl, M., Fürnrohr, B. G., Janko, C., Munoz, L. E., Voll, R. E., Gregory, C. D., Schett, G., and Herrmann, M. (2015) Loading of nuclear autoantigens prototypically recognized by systemic lupus erythematosus sera into late apoptotic vesicles requires intact microtubules and myosin light chain kinase activity. *Clin. Exp. Immunol.* **179**, 39–49 [CrossRef Medline](#)
29. Winau, F., Weber, S., Sad, S., de Diego, J., Hoops, S. L., Breiden, B., Sandhoff, K., Brinkmann, V., Kaufmann, S. H., and Schaible, U. E. (2006) Apoptotic vesicles crossprime CD8 T cells and protect against tuberculosis. *Immunity* **24**, 105–117 [CrossRef Medline](#)
30. Nagata, S., Hanayama, R., and Kawane, K. (2010) Autoimmunity and the clearance of dead cells. *Cell* **140**, 619–630 [CrossRef Medline](#)
31. Cerri, P. S. (2005) Osteoblasts engulf apoptotic bodies during alveolar bone formation in the rat maxilla. *Anat. Rec. A Discov. Mol. Cell. Evol. Biol.* **286**, 833–840 [Medline](#)
32. Ito, M., Amizuka, N., Nakajima, T., and Ozawa, H. (1999) Ultrastructural and cytochemical studies on cell death of osteoclasts induced by bisphosphonate treatment. *Bone* **25**, 447–452 [CrossRef Medline](#)
33. Eriksen, E. F., Melsen, F., and Mosekilde, L. (1984) Reconstruction of the resorptive site in iliac trabecular bone: a kinetic model for bone resorption in 20 normal individuals. *Metab. Bone Dis. Relat. Res.* **5**, 235–242 [CrossRef Medline](#)
34. Eriksen, E. F., Gundersen, H. J., Melsen, F., and Mosekilde, L. (1984) Reconstruction of the formative site in iliac trabecular bone in 20 normal individuals employing a kinetic model for matrix and mineral apposition. *Metab. Bone Dis. Relat. Res.* **5**, 243–252 [CrossRef Medline](#)
35. Tran Van, P., Vignery, A., and Baron, R. (1982) An electron-microscopic study of the bone-remodeling sequence in the rat. *Cell Tissue Res.* **225**, 283–292 [CrossRef Medline](#)
36. Dou, C., Li, J., Kang, F., Cao, Z., Yang, X., Jiang, H., Yang, B., Xiang, J., Xu, J., and Dong, S. (2016) Dual effect of cyanidin on RANKL-induced differentiation and fusion of osteoclasts. *J. Cell. Physiol.* **231**, 558–567 [Medline](#)